# BUOYANCY VORTEX POWER FROM LOW-TEMPERATURE HEAT: PROGRESS

N.A. Hawkes[1], R.G.J. Flay[1], J.E. Cater[2], M. MacDonald[1]

[1]Department of Mechanical Engineering, University of Auckland, New Zealand

[2]Department of Engineering Science, University of Auckland, New Zealand

nhaw121@aucklanduni.ac.nz

**Keywords:** *missing, please address*

## ABSTRACT

This paper is a progress report since NZGW 2018, describing laboratory results and a scaling or non-dimensionalisation of atmospheric buoyancy vortices for power generation. It is based on the Oberbeck-Boussinesq assumption and assumes that the vortex flows are pseudo-cyclostrophic and that a radial Richardson number can serve as a predictor of the onset of Kelvin-Helmholtz instability leading to a transition to a turbulent plume. This is used to locate the cold reservoir of the vortex when viewed as a heat engine. It permits the prediction of the behaviour of large vortices in the atmosphere by using data from experiments on small vortices.

## 1. INTRODUCTION

Atmospheric buoyancy vortices such as dust-devils, water-spouts and fire-whirls, are one instance of flows arising from rotating turbulent thermal convection (Horn and Aurnou, 2018, 2019). The use of an artificial vortex of this type as a source of carbon-neutral electricity generation is envisaged. Such vortices result from a combination of strong convection with rotation around the vertical axis (swirl). These properties are intermittent in the normal atmosphere, so natural vortices are transient. However steady-state convection and swirl can be engineered to produce continuous vortices. This has been demonstrated by others (Mullen and Maxworthy, 1977; Simpson and Glezer, 2016).

At an industrial scale, strong convection can be engineered, as shown schematically in Figure 1, by pumping water, taken from the secondary cooling circuits of existing thermal power stations, through nozzles to produce warm saturated airflows within the vortex core. The resulting convection of saturated air releases latent heat through condensation, which acts to increase the temperature difference from the vortex core to the environment as the core flows rise. This produces a vertical gradient of buoyancy which introduces vertical strain in the core-flows to act against radial diffusion and allows the core to rise to great height. Swirl is engineered using a ring of vertical aerofoils set around the heat-source. The angle of the aerofoils to the radial direction introduces swirl into the rising air drawn in by convection over the heat source. Swirl is then concentrated into the vortex core through the 'end-wall effect' arising from friction at the ground and conservation of angular momentum, acting on the vortex flows (Hawkes et al., 2018). This produces an area of high wind speeds at ground level, which can be used to drive a turbine for power generation.

This method allows for carbon-neutral power generation from existing waste heat flows in light- and nil-wind conditions. It could complement existing wind generation in that it allows for the 'wind-gap' in generation capacity experienced in light-wind conditions from conventional wind turbines to be reduced without grid-scale storage. It is expected to have low capital costs, as it does not require masts, deep foundations, large diameter turbines or high-torque gearboxes.

Preliminary analysis (Hawkes et al., 2018) suggests that such a Vortex Station with a 'swirl-henge' diameter of 20 m would produce a vortex of 2 m core diameter, allowing for 1 MWe of generation at a conversion efficiency from heat input to electrical output of the order of 5%. This is based on a modification of published heat-engine models (Renno et al., 1998; Renno and Bluestein, 2001) which assume that the cold reservoir of the heat engine is at the top of the vortex. The vortex-top is the area where the coherent vortex-core flows break down to a turbulent plume.

More accurate prediction of the flow scales and available power requires a non-dimensionalisation of the temperatures and forces of the vortex flows to allow laboratory results to be used to predict performance at larger scales in the atmosphere, as discussed in Section 3.

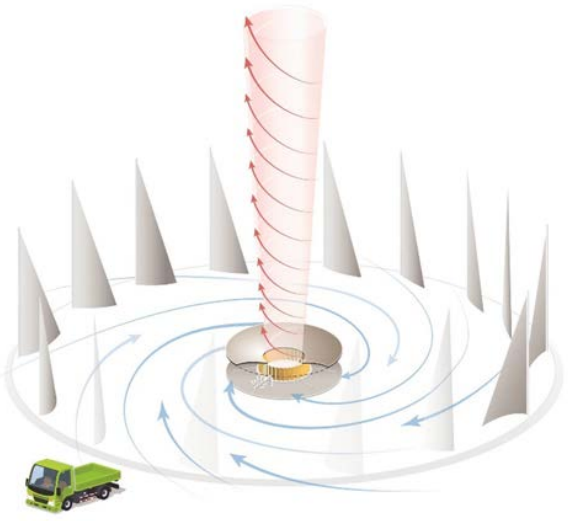

**Fig. 1 Outline Schematic of a 1 MWe Vortex Station (Vortex Power Systems Ltd.) showing a `swirl henge' of vanes around the vertical vortex.**

## 2. LABORATORY RESULTS

### 2.1 Experimental Cabinet

The Buoyancy Vortex Extension Cabinet is shown in Figure 2. Air is introduced into the cabinet at the base through vertical ducts of triangular section to minimise disruption from drafts in the wind-tunnel hall.

### 2.2 Heated Plate

The vortices are formed over a 1 m diameter, 16 mm thick aluminium hotplate with a 2.5 kW rated element, heating an area 700 mm in diameter.

### 2.3 Core Stabiliser

The circular baffle, seen in the centre of the hotplate in Figure 3, is used to impose axial symmetry on the rising vortex flows. The vortex was also seen to be stabilised against side winds, which were introduced by opening one side of the cabinet during experiments.

### 2.4 Turbine wheel

A cylindrical turbine wheel of 100 mm diameter with twelve 20 mm-tall vertical vanes rotating around the vertical axis of the experiment is set in the inflow zone above the hotplate, to investigate the interaction between the turbine and vortex. The turbine vanes can be seen below the core stabiliser in Figure 3. As is expected from considerations of radial continuity and the transfer of angular momentum to the turbine blades to produce shaft torque, the turbine acts to reduce the tangential velocity in the inflows, thus reducing swirl in the core. The rate of rotation of the turbine was measured using a high-speed camera to allow estimation of Froude number.

### 2.5 Short swirl vanes

The hotplate is encircled by swirl vanes shown in Figures 1 and 3, that can be set at 30º, 45º, 60º or 75º to the radial. The swirl vanes are shorter than those previously used (Mullen and Maxworthy, 1977; Simpson and Glezer, 2016). Little difference in vortex structure or height arising from using shorter vanes was found, except that the time taken for the vortex to self-organise is slightly longer. Figure 3 shows twelve vanes in 4 mm thick Perspex, 300 mm tall by 150 mm wide, set around a 1 m diameter hotplate. This suggests that the height of the swirl vanes is not a suitable vertical scale for non-dimensionalisation and is of practical importance for power generation since it shows that creating tall vortices does not require tall swirl vanes, taller being more expensive.

### 2.6 Heating at height

The use of saturated air flows in the core allows the use of infra-red heaters (6 off RS 196-6478 650W rated) as seen in Figure 5. Their radiation passes through the dry air around the core to preferentially heat the water vapour in the saturated core flows, thus allowing non-contact heating of the core at height to investigate extension of the vortex to greater aspect ratios.

### 2.7 Flow visualisation

Condensing water vapour is used for flow visualisation of the core. The water vapour is produced by dripping a solution of e-vape liquid in water onto the hotplate outside the core. As the vapour is carried into the lower pressure area of the core, saturation and condensation result. This gives very effective flow visualisation but complicates the instrumentation. It is planned to use ultrasonic anemometers mounted on the traverse rig to allow non-contact measurement of radial profiles of core density and tangential velocity at different heights.

Figure 3 shows a qualitative comparison of structures obtained in our experiments and the DNS results (Horn and Aurnou, 2019). Values of the gravitational Rossby number and Froude number in our experiment approximate those associated in the DNS with the transition from three-dimensional (3D) to QC, but at a slightly higher Rayleigh number. This suggests that cyclostrophic balance is the main determinant of vortex structure in the experiment.

**Fig. 2 Buoyancy Vortex Extension Cabinet, Wind-Tunnel Hall, University of Auckland.**

Figure 4 shows characteristic temperature fields from a direct numerical simulation (DNS) of Rotating Rayleigh-Benard convection (RRBC) (Horn and Aurnou, 2018) in terms of the non-dimensionalisation described in Section 3. Our experimental results fall within the quasi-cyclostrophic balance (QC) regime (area at bottom right). They show similar structures to those seen in the DNS in the QC regime, at similar values of Rossby number and Froude number.

The most apparent difference between RRBC and the experimental buoyancy vortices seen in Figure 3 is that the aspect ratio in the RRBC is set by the geometry of the rotating domain, while the aspect ratio of the experimental buoyancy vortex is set by the height at which the coherent core breaks down to a turbulent plume. The structure of experimental vortices formed above hotplates in the absence of heating at height is well determined in most respects (Mullen and Maxworthy, 1977; Simpson and Glezer, 2016), but the height of the vortex is not explained. It is found that vortex height can be extended by additional heating at height, which gives increased tangential velocities at the ground. This is of importance to the possibility of using a buoyancy vortex in the free atmosphere to drive a turbine.

In the absence of lapse-rate divergence, buoyancy vortex cores show a characteristic conical vortex structure with a constant cone angle for Rt,, i.e.

$$\frac{\partial Rt}{\partial z} = \text{constant}$$


ISSN 2703-4275


**Fig. 3 Comparison of flow structures in our experiments and in the DNS of RRBC Experiment Ra~109, Ro~1, Fr~0.5: DNS Ra=108, Ro=1, Fr=0.5 (Horn and Aurnou, 2018).**

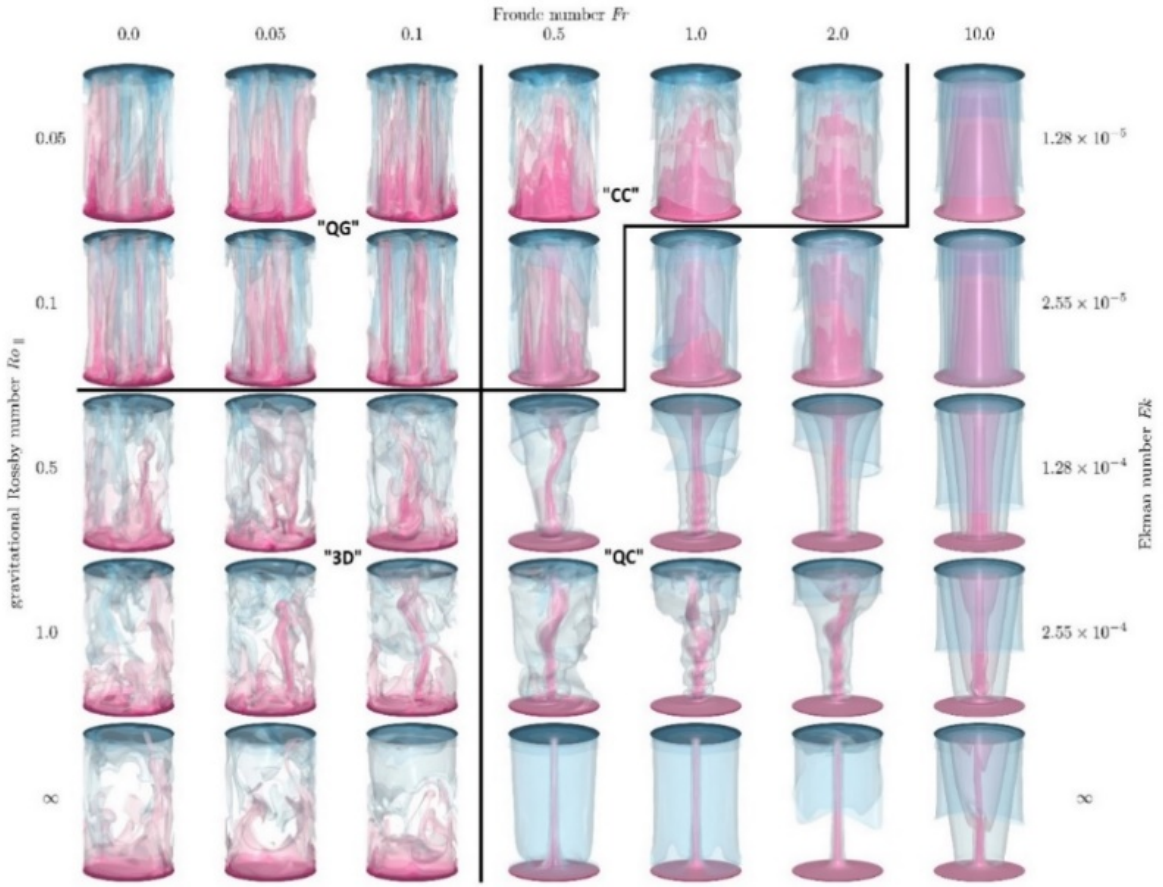


**Fig. 4 Regime diagram in the gravitational Rossby number to Froude number space for Ra=108, showing temperature fields in the three-dimensional (3D), quasi-geostrophic (QG), quasi-cyclostrophic (QC) and Coriolis, and centrifugal force (CC) regimes: adapted with permission from Horn and Aurnou (2018).**

where Rt is the radius of maximum tangential velocity and z is height (Simpson and Glezer, 2016). The same structure is evident in the present experiments, as shown in Figure 3. A discontinuity arising at the top of the vortex is observed involving a breakdown to a turbulent plume with an associated increase in entrainment and cone angle.

With infra-red heating the height of core breakdown to the plume was extended from ~1.5 m to ~2.5 m, with a smaller apparent cone angle and the turbine speed increased from 135 rpm to 163 rpm. In both cases, the power to hotplate = 2kW, 60º swirl vane angle, Ra~109, Ro~1, Fr~0.5. This preliminary result suggests that the height of core breakdown may be a suitable vertical length scale for non-dimensionalisation. The height of the swirl-vanes does not seem to be a suitable vertical length scale.

Initial estimates from our experiments suggest 〖Ri〗_r>0.25 at the base of the vortex and 〖Ri〗_r≅0.25 at the breakdown to the plume, as discussed in Section 3.1.1. Future work will investigate whether this condition can predict vortex height in the experiment. If so, it will allow a non-dimensionalisation for buoyancy vortices, using the height of core breakdown as the vertical length scale. This should enable the height of artificial vortices in the atmosphere to be predicted.

## 3. NON-DIMENSIONALISATION

Rotating Rayleigh-Benard convection (RRBC) has been widely used as a paradigm model of rotating turbulent thermal convection (Horn and Aurnou, 2018). RRBC laboratory experiments involve a fluid rotated around a vertical axis while being heated from below and cooled from above and has been widely studied (Horn and Aurnou, 2019). Although the boundary conditions are different, our experiments suggest the inner flows in RRBC and atmospheric buoyancy vortices are sufficiently similar that the non-dimensionalising ratios and quantities developed in studying RRBC may be applied to atmospheric buoyancy vortices, with some revision.

Previous authors (Horn and Aurnou, 2019) use a non-dimensionalising scheme progressing from the continuity (Eq 2a), the Navier-Stokes equations using the Oberbeck-Boussinesq approximation (Eq 2b) and the temperature Eq (2c) in Direct Numerical Simulations (DNS) of RRBC. The Oberbeck-Boussinesq approximation, considering density effects under strong gradients as well as buoyancy, is used to write a version of the Navier-Stokes equation that is suited to analysis of rotating turbulent thermal convection.

In the DNS (Horn and Aurnou, 2019) the domain is rotated about its vertical axis with angular velocity $\boldsymbol{\Omega} = \Omega\mathbf{e_z}$. The molecular kinematic viscosity $\nu$ and thermal diffusivity $\kappa$ are assumed to be constant for the fluid. Density is expressed as a Taylor expansion around the mean temperature:

$$\rho = \rho_m\big(1 - \alpha(T - T_m)\big), \quad \alpha \equiv -\frac{1}{\rho_m}\frac{\partial \rho}{\partial T} = \text{the isobaric expansion coefficient.} \tag{1}$$

The higher order term $\rho_m\alpha(T - T_m)$ is neglected except in the gradient terms for gravitational and centrifugal acceleration, resulting from buoyancy forces. The mean term $\rho_m$ is absorbed into the pressure term. The other terms are turbulent diffusion and Coriolis acceleration.

The governing equations are then written in cylindrical coordinates as:

$$\nabla.\mathbf{u} = 0 \tag{2a}$$

$$D_t\mathbf{u} = \nu\nabla^2\mathbf{u} - \nabla p + 2\Omega\mathbf{u}\times\mathbf{e}_z - \Omega^2 r\alpha(T - T_m)\mathbf{e}_r + g\alpha(T - T_m)\mathbf{e}_z \tag{2b}$$

$$D_t T = \kappa\nabla^2 T \tag{2c}$$

where $\boldsymbol{u}$ is the velocity vector, $\nu$ is the kinematic viscosity, $p$ is pressure, $r$ is radius within the vortex, $\alpha$ is the isobaric expansion coefficient, $T$ is absolute temperature, $\mathbf{e}_r$ and $\mathbf{e}_z$ are the radial and vertical unit vectors, and $\kappa$ is the thermal diffusivity.

The effect of the gravitational and centrifugal terms is to drive warmer, less dense air upwards and radially inwards. These equations are expressed in non-dimensional form as:

$$\nabla.\hat{\mathbf{u}} = 0 \tag{3a}$$

$$D_t\hat{\mathbf{u}} = \frac{Pr^{1/2}}{Ra^{1/2}\gamma^{3/2}}\nabla^2\hat{\mathbf{u}} - \nabla\hat{p} + \frac{\gamma^{\frac{1}{2}}}{Ro_g}\hat{\mathbf{u}}\times\mathbf{e}_z - Fr\,\hat{r}\,\hat{T}\,\mathbf{e}_r + \hat{T}\mathbf{e}_z \tag{3b}$$

$$D_t\hat{T} = \frac{1}{Ra^{1/2}Pr^{1/2}\gamma^{3/2}}\nabla^2\hat{T} \tag{3c}$$

Reference scales are used: the domain radius R, the imposed vertical temperature difference $\Delta$, and the velocity $V = \sqrt{\alpha g \Delta R}$, so $\hat{r} = r/R$, $\hat{T} = \frac{T - T_m}{\Delta}$, $\hat{\mathbf{u}} = \mathbf{u}/V$, $\hat{p} = p/\rho V^2$ and $\hat{t} = tV/R$. The boundary conditions are assumed to be no-slip on all walls, the sidewall adiabatic and the top and bottom boundaries isothermal at

$\hat{T}_{top} = -1/2$, $\hat{T}_{bottom} = 1/2$. The fluid layer height is H.

The input parameters of the DNS (Eq. 4) are:

- the Rayleigh Number: $Ra = \frac{\Gamma_d}{\Gamma_c}$, where $\Gamma_d$ is the timescale for thermal transport by diffusion and $\Gamma_c$ is the timescale for thermal transport by convection at velocity $V$,
- the Prandtl number of the fluid,
- the rotational Froude number, describing the importance of centrifugation.

$$Ra \equiv \frac{\alpha g \Delta H^3}{\kappa\nu} = \frac{\Gamma_d}{\Gamma_c}, \qquad Pr \equiv \frac{\nu}{\kappa}, \qquad Fr \equiv \frac{\Omega^2 R}{g} \tag{4}$$

Rotation is characterised using a gravitational Rossby number ($Ro_g$) derived from the relationship of rotation and inertia:

$$Ro_g \equiv \frac{\Gamma_\Omega}{\Gamma_{gb}} = \frac{\sqrt{\alpha g \Delta H}}{2\Omega H} \quad (5)$$

A centrifugal Rossby number is also derived:

$$Ro_c \equiv \frac{\Gamma_\Omega}{\Gamma_{cb}} = \frac{\sqrt{\alpha\Delta}}{2} = \sqrt{\frac{Ro_g^2.Fr}{\gamma}}, \quad \gamma \equiv \frac{R}{H} \quad (6)$$

where $\gamma$ is the aspect ratio of the domain.

The relevant timescales include:

$\Gamma_\Omega = \frac{1}{2\Omega}$, the Coriolis timescale,

$\Gamma_{gb} = \mathrm{T}_{ff} = \frac{H}{\sqrt{\alpha \mathrm{g} \Delta \mathrm{H}}}$, the gravitational buoyancy (or free-fall) timescale,

$\Gamma_{cb} = \frac{R}{\sqrt{\alpha \Delta \Omega^2 R^2}}$, the centrifugal buoyancy timescale.

Our vortices fall within the quasi-cyclostrophic regime (QC) as shown in Figure 4. This implies that centrifugal buoyancy dominates the flows within the QC regime and within our vortices.

### 3.1 Proposed Non-dimensionalisation for Buoyancy Vortices

Given that the height of the buoyancy vortex is not obviously connected to the radial scale or the height of the swirl vanes, a modification of the non-dimensionalisation presented in the DNS study (Horne and Aurnou, 2019) is suggested with the substitution of:

$$V = \sqrt{g\alpha\Delta_p H_p}, \quad (7)$$

for the reference velocity, where $H_p$ is the height of the breakdown to a plume and $\Delta_p$ is the difference in virtual temperature between the air entering the base of the vortex core and that entering the base of the plume. The base of the plume is taken to be the cold reservoir of the heat-engine driving the vortex flows. There is some support for this in the literature. An analysis of tangential wind-speeds in dust-devils (Hawkes and Flay, 2017) found a correlation where:

$$V_t \propto \sqrt{CAPE(H_s).H_s}, \quad (8)$$

where $H_s$ is the height of the superadiabatic layer in the atmosphere, this seems to also be the height of the core before breakdown (Hawkes and Flay, 2017). CAPE(Hs) is the Convectively Available Potential Energy available up to that height.

An analytic solution of the Navier-Stokes equation (Kuo, 1966) for a vortex rising in a saturated atmosphere of virtual potential temperature $\theta$ and depth $h$, under constant lapse-rate divergence produces a similar velocity scaling:

$$\frac{V}{h} \propto \beta = \left[\frac{g}{\theta}\frac{\partial\theta}{\partial z}\right]^{1/2} \approx \sqrt{(g/T \;\; \delta T/h)},$$

which is equivalent to:

$$V \propto \sqrt{g\alpha\Delta \mathrm{h}}. \quad (9)$$

The axial momentum within a buoyancy vortex was modelled as (Simpson and Glezer, 2016):

$$\frac{d}{dz}\int_0^\infty \rho\left(w^2 - \frac{1}{2}v^2\right) r\, dr = \int_0^\infty \rho g' r\, dr, \quad (10)$$

where $g' = ((\rho_\infty - \rho(r,z))/\rho_\infty)g$ is the gravitational acceleration or specific buoyancy.

A modification of this term is useful for taller vortices, where the atmospheric density varies with height:

$$g^*(z) = ((\rho(\infty,z) - \rho(r,z))/\rho(\infty,z))g \quad (11)$$

It then follows that:

$$\int_0^H g^*(z)\; dz = CAPE(H). \quad (12)$$

Equations 9 and 11 involve the idea of lapse-rate divergence, wherein the core flows cool more slowly in rising than the surrounding atmosphere, leading to lower density in the core than in the surroundings. This is consistent with the idea of CAPE, which is widely used in meteorology.

Lapse rate divergence arises in a dry vortex, such as a dust-devil, with a core rising at the adiabatic lapse-rate in a super-adiabatic environmental layer. It arises in a condensing vortex, such as a water-spout or tornado, with a core rising at the pseudo-adiabatic lapse-rate in a temperate atmosphere. Lapse rate divergence or core heating at height introduce axial strain in the vortex core that acts to concentrate it in rising, against the effects of entrainment and radial diffusion. Lapse rate divergence cannot easily be scaled down, so artificial heating at height becomes necessary in our experiment.

Since the diameter of heating under the hotplate does not seem to dictate the structure of the vortex it is proposed that the value of *R* used for non-dimensionalising should be taken as the radius of the swirl vanes, as used in previous work (Mullen and Maxworthy, 1977; Simpson and Glezer, 2016), although this makes comparisons with the DNS of RRBC more difficult (Horn and Aurnou, 2018, 2019).

#### 3.1.1 Richardson Number and Kelvin Helmholtz Instability

The Richardson Number (*Ri*) is widely used in studying geophysical flows to predict the onset of entrainment and turbulent mixing in shear flows under density gradients. It is a dimensionless number that expresses the ratio of buoyancy to the flow shear. In the study of these flows, instances with *Ri* > 0.25 are expected to be stable, breaking down at *Ri* = 0.25 via a Kelvin Helmholtz instability with subsequent production of turbulent energy (Renno and Bluestein, 2001).

If the vortex core flows are quasi-centrifugal, the point at which breakdown to the plume occurs should be predictable using a radial Richardson number. A transition at the top of the vortex is expected, similar to a Kelvin Helmholtz instability, leading to the production of turbulent energy and the creation of a turbulent plume immediately above the coherent vortex core. The Richardson number is given by:

$$\text{Radial Richardson Number} \equiv \frac{buoyancy}{flow\ shear} = Ri_r = \frac{a}{\rho}\frac{\frac{\partial \rho}{\partial r}}{\left(\frac{\partial v}{\partial r}\right)^2} \quad (13)$$

where $a = \frac{v^2}{r}$ is the centripetal acceleration, with the expectation that the breakdown to a plume may be associated with a condition $Ri_r \leq 0.25$. If the breakdown to the plume can be predicted in this way, this then allows estimation of $H_p$ and $\Delta_p$ to complete the non-dimensionalisation.

## 4. CONCLUSIONS

The characteristic and instantaneous flow fields in our experiments appear similar to those seen within the QC regime for similar values of ($Fr$,$Ro_g$) (Horn and Aurnou, 2018, 2019). The trends are also similar, with experimental vortex cores becoming slimmer, and less subject to transient instabilities at the higher Rossby and Froude numbers arising from increased hot-plate temperatures.

The height of the vortex does not exhibit a simple relationship with the radial dimensions in the experiment or the height of the swirl vanes. It seems to be the height of onset of vortex core breakdown to a turbulent plume, occurring at a height which may be predicted through the use of a radial Richardson number.

A modification of the reference scales for velocity, radius, height, and temperature difference used in a published non-dimensionalisation of Rotating Rayleigh-Benard convection is suggested. This modification will allow the prediction of the required heat-input power and temperature and vortex station size to generate an artificial atmospheric vortex that could drive a turbine to provide carbon-neutral power generation of a desired electrical power, based on experimental results at much smaller scale.

## REFERENCES


Horn S, Aurnou JM: Regimes of Coriolis-centrifugal convection. *Physical Review Letters* 120:204502 (2018)

Horn S, Aurnou JM: Rotating convection with centrifugal buoyancy: Numerical predictions for laboratory experiments. *Physical Review Fluids* 4:073501 (2019)

Mullen JB, Maxworthy T: A laboratory model of dust devil vortices. *Dynamics of Atmospheres and Oceans* 1:181-214 (1977)

Simpson MW, Glezer A: Buoyancy-induced, columnar vortices. *Journal of Fluid Mechanics* 804:712-748. (2016)

Hawkes NA, Flay RGJ, Cater JE: Buoyancy Vortex Power from Low-Temperature Heat. *Proc. 40th New Zealand Geothermal Workshop*, Taupo, New Zealand. (2018)

Renno N, Burkett M, Larkin MP: A simple thermodynamical theory for dust devils. *Journal of the Atmospheric Sciences*. 55:3244-3252 (1998)

Renno NO, Bluestein HB: A Simple Theory for Waterspouts. *Journal of the Atmospheric Sciences* 58:927. (2001)

Church C, Snow JT, Baker GL, Agee EM: Characteristics of tornado-like vortices as a function of swirl ratio: A laboratory investigation. *Journal of the Atmospheric Sciences* 36:1755-177. (1979)

Hawkes NA, Flay RGJ A Model of Tangential Wind-speeds in Dust-Devils. *9th Asia-Pacific Conference on Wind Engineering*, Auckland, New Zealand. (2017)

Kuo HL: On the dynamics of convective atmospheric vortices. *Journal of the Atmospheric Sciences* 23:25-42. (1966)